emission behaviors of RuL_3^{2+} and $RuL_2(CN)_2$ are necessary to fully understand the excited-state properties of these complexes.

Acknowledgment. This work was partly supported by a Grant-in-Aid for Scientific Research by the Ministry of Education, Science and Culture, Japan (61740247). We thank Drs. T. J. Meyer, E. Danielson, and R. S. Lumpkin for providing a preprint of ref 8 and to one of the reviewers for valuable comments.

Registry No. *cis*-$Ru(phen)_2(CN)_2$, 112087-85-1; *cis*-$Ru(phen)_2(CN)_2^+$, 112087-86-2; *cis*-$Ru(phen)_2(CN)_2^-$, 112087-87-3; *cis*-$Ru(phen)_2(CN)_2^{2-}$, 112087-88-4; KSCN, 333-20-0.

Contribution from the Department of Chemistry, Northern Illinois University, DeKalb, Illinois 60115

Vapor-Phase Electronic Absorption Spectra and Solution Magnetic Circular Dichroism and Absorption Spectra for Dihalo- and Halomethylmercury(II)

M. Meral Savas and W. Roy Mason*

Received July 9, 1987

Vapor-phase electronic absorption spectra in the UV region (3.0–5.2 μm^{-1}) are reported for HgI_2, $HgBr_2$, and $HgCl_2$ at temperatures between 130 and 150 °C and for CH_3HgI, CH_3HgBr, and CH_3HgCl at temperatures between 65 and 85 °C. Absorption and magnetic circular dichroism (MCD) spectra are also presented for room-temperature cyclohexane solutions of HgX_2, CH_3HgI, and CH_3HgBr. Several bands in the vapor-phase spectra of the iodo and bromo complexes reveal weak vibrational structure. In particular bands at 4.45 μm^{-1} for HgI_2 and 4.97 μm^{-1} for CH_3HgI show long progressions in the bending mode of the complex and indicate excitation to bound molecular excited states. The solution MCD spectra show two prominent positive pseudo *A* terms for the two lowest energy band systems at 3.62 and 4.47 μm^{-1} for HgI_2, and a similar positive pseudo *A* term is also found for the lowest band at 4.32 μm^{-1} for CH_3HgI. The absorption and MCD spectra for the iodo complexes are interpreted by means of a ligand to metal charge-transfer (LMCT) model involving states of the $I^- \rightarrow Hg$ 6s excited configurations. The model includes the effects of halide spin–orbit coupling on the excited LMCT states and can account for differences observed between the absorption intensity and MCD pattern for the iodo complexes and for the bromo complexes.

Introduction

Dihalo- and halomethylmercury(II) complexes, HgX_2 and CH_3HgX, X = Cl^-, Br^-, and I^-, exhibit linear two-coordination both in the vapor and in a variety of solution environments.[1] In spite of this simple coordination geometry and the closed-shell diamagnetic $5d^{10}$ electronic configuration of Hg(II), the description of the lowest energy excited electronic states of these compounds and the assignment of their UV spectra has been lacking in detail and is not free of disagreement. This situation may be partly due to some experimental difficulties in obtaining reliable spectroscopic data under conditions where the two-coordinate species are well-defined. For example, there have been a number of solution spectral studies for HgX_2 in a wide range of solvents[2-6] (comparatively few have been reported for CH_3HgX[7,8]). However, the interpretation of these spectra may be questioned in some cases because dissociation occurs in aqueous solutions in the absence of added halide[5] and the solubility is low in nonaqueous solvents, where solvolysis can also be a complication if the solvent is a potential ligand (e.g. alcohols, acetonitrile, ethers, etc.). In the presence of added halide, species such as HgX_3^- or HgX_4^{2-} form and free halide absorptions tend to dominate the UV spectra in the region 250–190 nm. Further, spectra obtained for HgX_2 in aromatic solvents show differences compared to those obtained in nonaromatic solvents, and these differences have been interpreted as the formation of intermolecular solvent–HgX_2 charge-transfer complexes in the aromatic solvents.[1f,2] All of these complications are expected to lead to Beer's law failure and make questionable any interpretation based on simple linear HgX_2 or CH_3HgX species. In the vapor the simple complexes should be well-defined, but because of their low vapor pressure, elevated temperature and long-path cells are required to obtain reasonable spectra in the UV region.

The solution difficulties notwithstanding, the lowest energy bands for HgI_2, $HgBr_2$, and $HgCl_2$ in nonaromatic hydrocarbon solvents (where complications appear to be minimized) are found near 266, 225, and 200 nm, respectively. A similar blue shift from CH_3HgI to CH_3HgBr to CH_3HgCl has also been observed in methanol,[8] but Beer's law compliance and lack of solvolysis was not reported. The blue shift from I^- to Cl^- has been offered as evidence for a ligand to metal charge-transfer (LMCT) process.[4-6] Consistent with this assignment, photoelectron spectra for HgX_2 and CH_3HgX show that the lowest energy ionizations (9–14 eV) are from the halo ligands.[9] Ionization from the Hg(II) 5d orbitals is found at higher energy (>15 eV). Even though the LMCT assignment of the UV spectra seems reasonable, there remains disagreement as to detail. For example, the lowest energy bands in HgX_2 (and also in several mixed dihalo complexes HgXY) have been assigned as $^1\Sigma_g^+ \rightarrow {}^1\Delta_u$, a halide to Hg(II) 6p LMCT.[4,6] Since a transition to a $^1\Delta_u$ state is electric-dipole-forbidden in $D_{\infty h}$, the observed intensities ($\epsilon \approx$ 1000–3000 M^{-1} cm^{-1}) were explained by assuming a bent (C_{2v}) upper state ($^1\Delta_u$ correlates with an electric-dipole-allowed $^1B_2$ state in C_{2v} symmetry). However, some recent MO calculations[10] that utilized a relativistic core potential for Hg(II) have been used to interpret the two lowest energy absorption bands in $HgCl_2$ and $HgBr_2$ as dipole-allowed LMCT to $^1\Pi_u$ and $^1\Sigma_u^+$ states of halide to Hg 6s configurations. The

(1) See for example: (a) Klemperer, W.; Lindeman, L. *J. Chem. Phys.* **1956**, *25*, 397. (b) Buchler, A.; Stauffer, J. L.; Klemperer, W. *J. Am. Chem. Soc.* **1964**, *86*, 4544. (c) Buchler, A.; Stauffer, J. L.; Klemperer, W. *J. Chem. Phys.* **1964**, *40*, 3471. (d) Gordy, W.; Sheridan, J. *J. Chem. Phys.* **1954**, *22*, 92. (e) Meic, Z.; Randic, M. *J. Mol. Spectrosc.* **1971**, 39. (f) Cheng, C. L.; Pierens, R. K.; Radford, D. V.; Ritchie, G. L. D. *J. Chem. Phys.* **1973**, *59*, 5209.
(2) Eliezer, I.; Avinur, P. *J. Chem. Phys.* **1971**, *55*, 2300.
(3) Eliezer, I.; Avinur, P. *J. Chem. Soc., Faraday Trans. 2* **1974**, *70*, 1316.
(4) Griffiths, T. R.; Anderson, R. A. *J. Chem. Soc., Faraday Trans. 2* **1979**, *75*, 957.
(5) Spiro, T. G.; Hume, D. N. *J. Am. Chem. Soc.* **1961**, *83*, 4305.
(6) Griffiths, T. R.; Anderson, R. A. *J. Chem. Soc., Dalton Trans.* **1980**, 209.
(7) Gowenlock, B. G.; Trotman, J. *J. Chem. Soc.* **1955**, 1454.
(8) Goggin, P. L.; Hurst, N. W. *J. Chem. Res., Synop.* **1978**, 388.
(9) Eland, J. H. D. *Int. J. Mass. Spectrom. Ion Phys.* **1970**, *4*, 37.
(10) Wadt, W. R. *J. Chem. Phys.* **1980**, *72*, 2469.

0020-1669/88/1327-0658$01.50/0

LMCT states of the halide to Hg 6p configurations were calculated to be at least 2–3 eV higher in energy, owing primarily to the 5–6-eV 6s–6p atomic orbital separation. These calculations were also effective in providing an interpretation of the photodissociative properties of HgX_2, which are believed to be of key importance in Hg(II) excimer lasers.[10]

A number of vapor-phase spectral measurements have been reported for HgX_2,[11-17] but surprisingly none have been reported for CH_3HgX. Early studies for HgX_2 were concerned with structured intense band systems at high energy near 170, 184, and 208 nm for $HgCl_2$, $HgBr_2$, and HgI_2, respectively.[11] From analyses of the vibrational structure for $HgCl_2$ it was concluded that the transition was an allowed $^1\Sigma_g^+ \rightarrow {}^1\Sigma_u^+$ and that the $^1\Sigma_u^+$ excited state remained linear. These early studies did not identify the transition type or the excited configuration. The recent MO calculations[10] suggest a LMCT transition from halide to Hg $p\pi$ for these high-energy bands. More recent vapor-phase measurements were made between 290 and 190 nm, where unstructured lower energy bands analogous to those found in solution were observed.[15-17] A LMCT assignment was offered on the basis of the ordering of the lowest energy bands $I^- < Br^- < Cl^-$, but excited configurations and individual states were not identified.

Finally, another deficient aspect of the spectral interpretation and electronic structure of HgX_2 has been the neglect of halogen spin–orbit coupling. Even the relativistic core potential MO calculations[10] did not include halogen spin–orbit coupling. While neglecting ligand spin–orbit effects may not be serious for chloro complexes, the effects for bromo and especially iodo complexes will be significant ($\zeta_{np} \simeq 587$, 2457, and 5069 cm^{-1} for Cl, Br, and I, respectively[18]). Spin–orbit effects are clearly seen in the halogen ionizations in the photoelectron spectra of both HgX_2 and CH_3HgX.[9] The consequence of strong spin–orbit coupling in LMCT states for bromo and iodo complexes will be to make transitions to formally spin-forbidden triplet states more intense and thus prominent among the lowest energy absorptions of the complex.

Therefore, in order to further the understanding of the lowest energy excited states and the electronic structural details of the HgX_2 and CH_3HgX complexes, we have remeasured and report herein the vapor-phase spectra for HgX_2 between 130 and 150 °C in the region 3.0–5.2 μm^{-1} (330–190 nm). We have also obtained some vapor-phase spectra for CH_3HgX between 65 and 85 °C in the same spectral region. For the iodo and bromo complexes vibrational structure is observed in several of the low-energy bands. Finally, in an effort to provide some additional data to characterize low-energy states in solution, some absorption and magnetic circular dichroism (MCD) spectra for HgX_2, CH_3HgBr, and CH_3HgI in cyclohexane are reported herein.

Experimental Section

The CH_3HgX, X = Cl^-, Br^-, and I^-, compounds were purchased from Alfa/Ventron and were resublimed before use; they gave satisfactory elemental analyses. The mercury(II) halides $HgCl_2$, $HgBr_2$, and HgI_2 were of reagent grade. Vapor-phase electronic spectra were measured by means of a Cary 1501 spectrophotometer using 10.00-cm quartz cells. Elevated temperatures were maintained either by circulating hot water through a thermostated cell holder or by resistance heating a coil of wire wrapped about the cell. A calibrated thermocouple was attached to the cell to monitor the temperature. Solution absorption and MCD spectra were measured simultaneously and synchronously along the same light path by means of a computer-controlled spectrometer described earlier.[19] The MCD spectra were determined at 7 T by using a superconducting magnet system (Oxford Instruments SM2-7, fitted with a room-temperature bore tube). Spectral grade solvents were used throughout. All solution spectra were corrected for the solvent blank and were checked for Beer's law compliance.

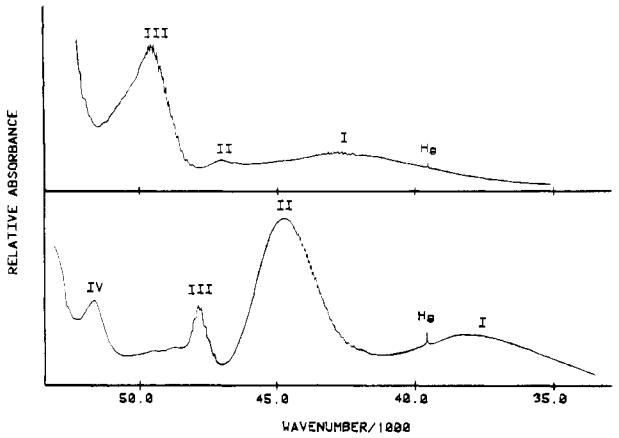

Figure 1. Vapor-phase absorption spectra (10.00-cm path) for HgI_2 at 130 °C (lower curve) and CH_3HgI at 65 °C (upper curve). The weak line at 3.9424 μm^{-1} is due to a trace elemental Hg impurity.

Results and Discussion

Vapor-Phase Absorption Spectra. The vapor-phase spectra obtained for HgI_2 and CH_3HgI are shown in Figure 1 (the 3.9424-μm^{-1} resonance line observed in each labeled "Hg" is due to a trace of elemental Hg in the vapor that could not be removed by sublimation). Bands II and III for HgI_2 and bands I, III, and IV (rising absorption toward high energy) for CH_3HgI clearly show weak vibrational structure on the otherwise broad bands. Some even weaker poorly resolved structure was also noted in the vapor-phase spectra of $HgBr_2$ and CH_3HgBr. No structure could be resolved in the spectrum of $HgCl_2$, and no well-defined bands were found below 5.2 μm^{-1} for CH_3HgCl. Band positions of the vibrational features and relative absorbances of the vapor-phase spectra are collected in Table I.

The structured band II of HgI_2 shows an average spacing between 25 vibrational features of 79 ± 8 cm^{-1} (II-5–II-29, Table I), except at the low-energy foot of the band, where the spacing is larger (~200 ± 60 cm^{-1}, II-1–II-4). Band III of HgI_2 shows an average spacing of 140 ± 30 cm^{-1} among six members across the band. Band II of $HgBr_2$ shows more poorly resolved features with an average separation of 225 ± 100 cm^{-1} between five features. The ground-state vibrational frequencies from Raman and IR spectra[20] for HgI_2 and $HgBr_2$, respectively, are ν_1'' (σ_g^+) = 158, 219 cm^{-1}, ν_2'' (π_u) = 63, 73 cm^{-1}, and ν_3'' (σ_u^+) = 237, 294 cm^{-1}. Thus, the structure in band III of HgI_2 and band II of $HgBr_2$ is likely due to progressions in the totally symmetric excited-state mode ν_1', with frequencies slightly reduced from their ground-state values. The structure in band II of HgI_2 consists of a long 79-cm^{-1} progression that is too low in frequency to be ν_1'. This progression could be due to $2\nu_2'$, a double excitation of a linear excited-state bending mode with frequency reduced from the ground-state value. Alternatively the progression could arise from a single excitation in the bending mode of a bent excited state (ν_2, has A_1 symmetry in C_{2v}), but this would require a higher excited-state frequency than for the ground-state bending mode. In either case a large shift of the excited-state potential surface relative to the ground state in the Franck–Condon approximation is implied. The larger, rather anharmonic spacing between vibrational features at the foot of band II may signal the presence of another electronic state. However, an alternative possibility is that these features are due to simultaneous excitation of ground-state vibrations (hot bands). This latter possibility is reasonable since kT at the temperature of the vapor-phase measurements approaches 300 cm^{-1}. If hot bands are present, the vibrational origin of band II is estimated to be near 4.257 μm^{-1},

(11) See ref 10 for a discussion of early vapor-phase spectra for HgX_2.
(12) Bell, S.; McKenzie, R. D.; Coon, J. B. *J. Mol. Spectrosc.* **1966**, *20*, 217.
(13) Bell, S. *J. Mol. Spectrosc.* **1967**, *23*, 98.
(14) Gedanken, A.; Raz, B.; Even, U.; Eliezer, I. *J. Mol. Spectrosc.* **1969**, *32*, 287.
(15) Maya, J. *J. Chem. Phys.* **1977**, *67*, 4976.
(16) Roxlo, C.; Mandl, A. *J. Appl. Phys.* **1980**, *51*, 2969.
(17) Templet, P.; McDonald, J. R.; McGlynn, S. P. *J. Chem. Phys.* **1972**, *56*, 5746.
(18) Jørgensen, C. K. *Mol. Phys.* **1959**, *2*, 309.
(19) Mason, W. R. *Anal. Chem.* **1982**, *54*, 646.
(20) Loewenschuss, A.; Ron, A.; Schnepp, O. *J. Chem. Phys.* **1969**, *50*, 2502.

Table I. Vapor-Phase Spectral Data[a]

band no.	$\bar{\nu}$, μm^{-1}	rel abs	band no.	$\bar{\nu}$, μm^{-1}	rel abs	band no.	$\bar{\nu}$, μm^{-1}	rel abs
				$HgBr_2$[b]				
I	4.370	0.219	II-2	5.030[c]	0.982	II-4	5.080[c]	0.982
II-1	5.020[c]	0.945	II-3	5.060	1.000	II-5	5.110[c]	0.927
				HgI_2[d]				
I	3.780	0.417	II-14	4.340	0.642	II-28	4.453	1.000
II-1	4.190[c]	0.298	II-15	4.348	0.675	II-29	4.460	1.000
II-2	4.215[c]	0.305	II-16	4.357	0.722	II-30	4.605[c]	0.417
II-3	4.237[c]	0.331	II-17	4.365	0.748	II-31	4.616[c]	0.351
II-4	4.250[c]	0.351	II-18	4.373	0.795	II-32	4.630[c]	0.285
II-5	4.257[c]	0.371	II-19	4.381	0.815	II-33	4.643[c]	0.232
II-6	4.272[c]	0.387	II-20	4.389	0.848	III-1	4.745[c]	0.212
II-7	4.280[c]	0.424	II-21	4.397	0.874	III-2	4.750[c]	0.238
II-8	4.290[c]	0.450	II-22	4.405	0.901	III-3	4.765	0.318
II-9	4.300[c]	0.490	II-23	4.414	0.933	III-4	4.781	0.404
II-10	4.310[c]	0.509	II-24	4.421	0.947	III-5	4.795	0.424
II-11	4.317[c]	0.556	II-25	4.430	0.967	III-6	4.805	0.364
II-12	4.325[c]	0.569	II-26	4.438	0.980	IV	5.185	0.424
II-13	4.334[c]	0.603	II-27	4.445	0.993			
				CH_3HgBr[e]				
I	4.650[c]	0.269	II-5	5.000[c]	0.636	II-10	5.120[c]	0.985
II-1	4.940[c]	0.513	II-6	5.010[c]	0.656	II-11	5.220	1.000
II-2	4.950[c]	0.528	II-7	5.035[c]	0.718	II-12	5.255[c]	0.959
II-3	4.964[c]	0.559	II-8	5.065[c]	0.779	II-13	5.285[c]	0.897
II-4	4.975[c]	0.585	II-9	5.095[c]	0.831	II-14	5.330[c]	0.785
				CH_3HgI[f]				
I-1	4.220	0.211	III-2	4.815	0.170	III-16	4.995[c]	0.937
I-2	4.235	0.214	III-3	4.835	0.207	III-17	5.010[c]	0.883
I-3	4.250	0.216	III-4	4.855	0.272	III-18	5.020[c]	0.828
I-4	4.265	0.219	III-5	4.875	0.371	III-19	5.030[c]	0.785
I-5	4.275	0.225	III-6	4.885	0.441	III-20	5.040[c]	0.747
I-6	4.290	0.225	III-7	4.905	0.610	III-21	5.050[c]	0.714
I-7	4.300	0.223	III-8	4.915	0.698	III-22	5.060[c]	0.681
I-8	4.315	0.223	III-9	4.925	0.774	III-23	5.070[c]	0.649
I-9	4.325	0.219	III-10	4.935	0.986	III-24	5.080[c]	0.621
I-10	4.355	0.219	III-11	4.945	0.948	III-25	5.095[c]	0.589
I-11	4.350	0.219	III-12	4.955	0.975	III-26	5.110[c]	0.523
I-12	4.360	0.218	III-13	4.965	1.000	IV-1	5.190[c]	0.556
II	4.690	0.188	III-14	4.975	1.000	IV-2	5.210[c]	0.703
III-1	4.800	0.154	III-15	4.985	0.975	IV-3	5.230[c]	0.959
				$HgCl_2$[g]				
I	5.000[c]	1.36						
				CH_3HgCl[h]				
				no maxima or shoulders below 5.2 μm^{-1}				

[a] 10.00-cm path. [b] 145 °C. [c] Shoulder. [d] 130 °C. [e] 90 °C. [f] 80 °C. [g] 150 °C. [h] 85 °C.

but it is difficult to be precise or to justify a more extensive analysis in view of the low resolution of the individual vibrational components. However, an important conclusion from the observation of vibrational structure in bands II and III is that the electronic transitions terminate in bound molecular excited states rather than dissociated states. This point will be considered again when the nature of these excited states are discussed below.

The structure observed near the maximum of the broad band I of CH_3HgI has an average spacing of 127 ± 26 cm^{-1} among 12 members, while the more prominent features of band III show spacing of 108 ± 19 cm^{-1} among 19 members (III-8–III-26; bands III-17–III-26 are poorly resolved). At the foot of band III 8 bands show a larger separation of 179 ± 39 cm^{-1} (III-1–III-8), similar to the case for band II of HgI_2. The increasing absorbance of band IV at high energy shows 3 features with a spacing of 200 cm^{-1}. Band II in CH_3HgBr shows 4 low-energy features with a spacing of ~117 ± 20 cm^{-1} (II-1–II-4) and 10 features across the band maximum with spacing ~300 ± 90 cm^{-1} (II-5–II-14), but the low resolution obtained limits the precision. A comparison of the observed features with ground-state frequencies (ν_4'' (σ^+) Hg–X stretch is 181 or 228 cm^{-1} and ν_8'' (π) C–Hg–X bend is 112 or 121 cm^{-1} for CH_3HgI or CH_3HgBr[21]) suggests long ν_8' bending progressions in bands I and III, with ν_4'' hot bands at the foot of band III for CH_3HgI. The larger frequency spacing near the band II maximum in CH_3HgBr suggests a ν_4' Hg–Br stretching progression, while ν_8' may be responsible for the low-energy features in this band. It is clear once again that these structured bands correspond to molecular excited states with the Hg–X bond intact because the other vibrations of these molecules involving the CH_3 or Hg–C are of significantly higher frequency (530–3000 cm^{-1} for the Hg–C stretching mode, CH_3 rocking modes, and C–H stretching modes[21]).

Solution MCD and Absorption Spectra. Figures 2 and 3 present MCD and absorption spectra for HgX_2, CH_3HgI, and CH_3HgBr in cyclohexane solution. Substantially the same results were also obtained for HgX_2 in methylcyclohexane solution. No spectral features were observed for CH_3HgCl below the solvent cutoff (5.0 μm^{-1}); acetonitrile solutions of CH_3HgCl were also investigated to 5.2 μm^{-1} with the same result. Quantitative spectral data for cyclohexane solutions are summarized in Table II.

The patterns of the MCD spectra in the region of band I for both HgI_2 and CH_3HgI are similar and give the appearance of a symmetrical positive A term.[22] In both cases however the $\Delta\epsilon_M$

(21) Goggin, P. L.; Kemeny, G.; Mink, J. *J. Chem. Soc., Faraday Trans. 2* **1976**, *72*, 1025.

(22) For a detailed description of MCD terms as well as the theory and conventions in standard use see: Piepho, S. B.; Schatz, P. N. *Group Theory in Spectroscopy with Applications to Magnetic Circular Dichroism*; Wiley-Interscience: New York, 1983.

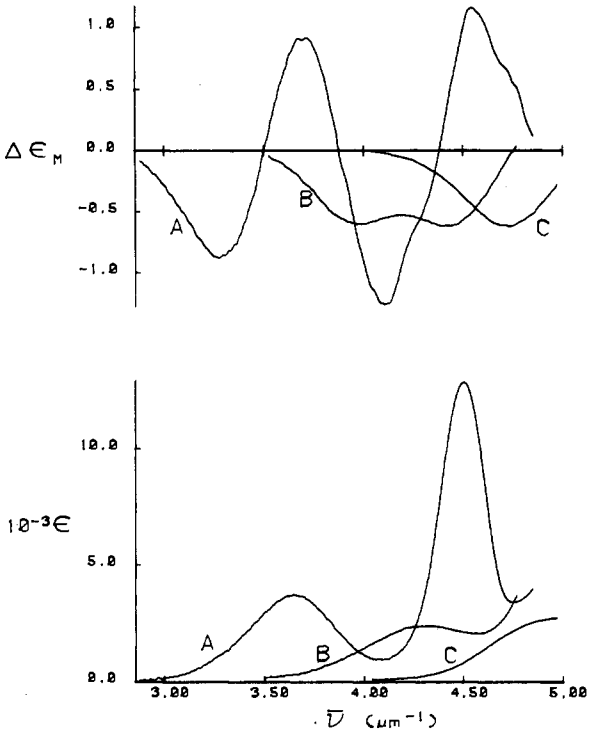

Figure 2. Electronic absorption (lower curves) and MCD (upper curves) spectra for cyclohexane solutions of HgI_2 (A), $HgBr_2$ (B), and $HgCl_2$ (C).

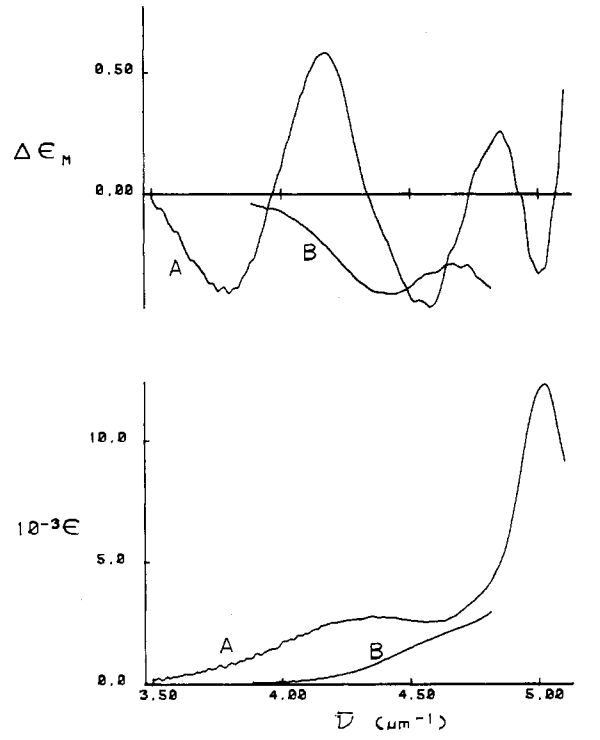

Figure 3. Electronic absorption (lower curves) and MCD (upper curves) spectra for cyclohexane solutions of CH_3HgI (A) and CH_3HgBr (B).

= 0 points (at 3.48 and 3.94 μm^{-1} for HgI_2 and CH_3HgI, respectively) differ significantly from the absorption maxima (at 3.62 and 4.32 μm^{-1}, respectively). This difference signals an underlying complexity of the broad absorption bands, which may include more than one unresolved transition. The MCD spectrum in the region of band II for HgI_2 also has the appearance of a positive *A* term, but again the $\Delta\epsilon_M = 0$ point (4.34 μm^{-1}) differs from the absorbance maximum (4.47 μm^{-1}). For CH_3HgI a second positive *A* term centered at 4.67 μm^{-1} appears below the energy of the solution band III. A precise term assignment is difficult in the absence of a resolved absorption feature, but in this case there is some broadness on the low-energy side of band III suggesting a poorly resolved shoulder near 4.67 μm^{-1}. Band III of CH_3HgI in solution at 4.97 μm^{-1} has associated with it a prominent negative MCD minimum at 4.95 μm^{-1}, but the MCD goes toward positive values just above the band maximum, suggesting yet another positive *A* term. A definite MCD term assignment, however, is precluded by the solvent cutoff. Finally, for $HgBr_2$, $HgCl_2$, and CH_3HgBr broad MCD minima are observed that differ in energy from the absorption maxima. However, in each case the lowest energy MCD feature is negative and appears at lower energy than the absorption maximum and in this respect the features are similar to the lowest energy MCD features of HgI_2 and CH_3HgI.

Table II. Spectral Data for Cyclohexane Solutions

band no.	λ, nm	$\bar{\nu}$, μm^{-1}	ε, M^{-1} cm^{-1}	$\bar{\nu}$, μm^{-1}	$\Delta\epsilon_M$, M^{-1} cm^{-1} T^{-1}
			$HgCl_2$		
I	202.4	4.94	2800[a]	4.68	−0.61
			$HgBr_2$		
I	234.2	4.27	2400	3.94	−0.60
II	198.0	5.05	13000	4.37	−0.61
			HgI_2		
				3.25	−0.88
I	276.1	3.62	3800	b 3.48	0
				3.67	+0.90
				4.07	−1.26
II	223.8	4.47	13000	b 4.34	0
				4.50	+1.16
			CH_3HgCl		
	no maxima or shoulders below 5.2 μm^{-1} [c]				
			CH_3HgBr		
I	216.1	4.63	2260[a]	4.38	−0.41
			CH_3HgI		
				3.77	−0.41
				b 3.94	0
				4.13	+0.58
I, II	231.7	4.32	2800	4.50	−0.44
				b 4.67	0
				4.77	+0.23
III	201.1	4.97	12000	4.95	−0.51

[a] Shoulder. [b] *A* term. [c] Cyclohexane solvent cutoff was ~5.0 μm^{-1}; CH_3CN solvent was also used (cutoff >5.2 μm^{-1}).

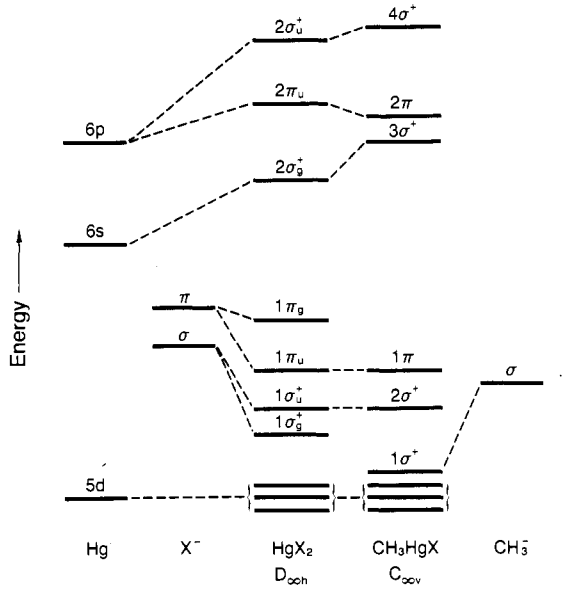

Figure 4. Simplified molecular orbital energy level scheme for HgX_2 and CH_3HgX.

Excited States and MCD Terms. In order to provide a basis for interpreting the MCD and absorption spectra, Figure 4 presents

Table III. Excited Configurations and States

excited config[a]		no spin–orbit coupling[b]	spin–orbit states[b,c]
HgX_2	CH_3HgX		
$(1\pi_u)^3(2\sigma_g^+)$	$(1\pi)^3(3\sigma^+)$	$^1\Pi_u$	Π_u
		$^3\Pi_u$	Π_u
			Σ_u^+
			(Σ_u^-, Δ_u)
$(1\sigma_u^+)(2\sigma_g^+)$	$(2\sigma^+)(3\sigma^+)$	$^1\Sigma_u^+$	Σ_u^+
		$^3\Sigma_u^+$	Π_u

[a] Notation as in Figure 4. Ground states: $...(1\sigma_u^+)^2(1\pi_u)^4(1\pi_g)^4$, $^1\Sigma_g^+$; $...(2\sigma^+)^2(1\pi)^4$, $^1\Sigma^+$. Filled orbitals are omitted, and parity-forbidden excited configurations, such as $(1\pi_g)^3(2\sigma_g^+)$, are not included. [b] Parity subscript is omitted for $C_{\infty v}$ states. [c] Dipole-forbidden states in parentheses.

a MO energy level scheme for the $D_{\infty h}$ HgX_2 and $C_{\infty v}$ CH_3HgX complexes. This scheme is constructed with the assumption that the highest occupied MO's are primarily X^- np orbitals. On the basis of photoionization spectra[9] the Hg 5d orbitals are placed lower in energy and to a first approximation are assumed to be part of the Hg^{2+} "core". The z axis in each case is taken to be the molecular axis, and the highest energy filled orbital is $1\pi_g$ or 1π, giving a $^1\Sigma_g^+$ or a $^1\Sigma^+$ diamagnetic ground state. The lowest energy excited configurations are expected to be of LMCT type and are assumed to involve the empty $2\sigma_g^+$ or $3\sigma^+$ orbital, which is primarily the Hg 6s orbital. Excited configurations involving the Hg 6p π levels are expected to be higher in energy on the basis of the earlier MO calculations.[10] Table III lists the LMCT states of the $2\sigma_g^+$ or $3\sigma^+$ excited configurations. In this table and in the discussion that follows here the $D_{\infty h}$ symmetry irrep designations are used. For the $C_{\infty v}$ symmetry irreps the parity subscript "u" is omitted. Dipole selection rules permit allowed transitions to Σ_u^+ (z polarized) and Π_u (x, y polarized) states. In the presence of strong spin–orbit coupling the Σ_u^+ and Π_u states of spin-forbidden triplet parentage will become intermixed with singlet states, and thus transitions to them may acquire considerable intensity. Table III also lists the spin–orbit states, denoted by the lack of spin multiplicity superscripts, which result from the singlet and triplet zero-order states. It should be noted that to a first approximation the spin–orbit interaction is entirely from the halide ligand because the Hg 6s orbital ($2\sigma_g^+$ or $3\sigma^+$) is unaffected by Hg spin–orbit effects. The Σ_u^+ and Π_u spin–orbit states can be determined in terms of the singlet and triplet states in the absence of coupling and are given by eq 1 and 2. The mixing coefficients

$$|\Pi_u(j)\rangle = a_j|^1\Pi_u\rangle + b_j|^3\Pi_u\rangle + c_j|^3\Sigma_u^+\rangle \quad (1)$$

$$|\Sigma_u^+(j)\rangle = d_j|^3\Pi_u\rangle + e_j|^1\Sigma_u^+\rangle \quad (2)$$

a_j–e_j are determined by diagonalizing the secular determinants in eq 3 and 4. In eq 3 and 4, the energies of the singlet and triplet

$$\begin{vmatrix} ^1\Pi_u - E & {}^1/_2\zeta & -{}^1/_2{}^{1/2}\zeta \\ {}^1/_2\zeta & ^3\Pi_u - E & -{}^1/_2\zeta \\ -{}^1/_2{}^{1/2}\zeta & -{}^1/_2\zeta & ^3\Sigma_u^+ - E \end{vmatrix} = 0 \quad (3)$$

$$\begin{vmatrix} ^3\Pi_u + {}^1/_2\zeta - E & -\zeta \\ -\zeta & ^1\Sigma_u^+ - E \end{vmatrix} = 0 \quad (4)$$

zero-order states appear along the diagonal and $\zeta = \zeta_{np}$ for the halide ligand. The elements of these determinants are determined by approximating the MO's as pure np halide and Hg 6s atomic orbitals.

Since the ground state of HgX_2 or CH_3HgX is nondegenerate, only A and B terms[22] are expected in the MCD (C terms will be absent). A terms originate from Zeeman splitting of degenerate states by the external magnetic field and therefore may be observed only for Π_u states. However, both Π_u and Σ_u^+ states may exhibit B terms, which result from excited-state mixing by the field. For the space-averaged case appropriate for HgX_2 or CH_3HgX in solution, the magnitudes of these terms are determined by the $\bar{A}_1$ and $\bar{B}_0$ parameters[22] given in eq 5–7, where μ_B is the Bohr

$$\bar{A}_1(\Pi_u(j)) = -\left(\frac{1}{2^{1/2}\mu_B}\right)\langle\Pi_u(j)||\mu^{\Sigma_g^-}||\Pi_u(j)\rangle\bar{D}_0(\Pi_u(j)) \quad (5)$$

$$\bar{B}_0(\Pi_u(j),\Pi_u(k)) = \mathrm{Re}\left(\frac{-2}{3(2^{1/2})\mu_B}\sum_{k\neq j}\frac{\langle\Pi_u(j)||\mu^{\Sigma_g^-}||\Pi_u(k)\rangle}{\Delta W_{kj}}\langle\Sigma_g^+||m^{\Pi_u}||\Pi_u(j)\rangle \times \langle\Pi_u(k)||m^{\Pi_u}||\Sigma_g^+\rangle\right) \quad (6)$$

$$\bar{B}_0(\Sigma_u^+(j),\Pi_u(k)) = \mathrm{Re}\left(\frac{2}{3\mu_B}\sum\frac{\langle\Sigma_u^+(j)||\mu^{\Pi_u}||\Pi_u(k)\rangle}{\Delta W_{kj}}\langle\Sigma_g^+||m^{\Sigma_u^+}||\Sigma_u^+(j)\rangle \times \langle\Pi_u(k)||m^{\Pi_u}||\Sigma_g^+\rangle\right) \quad (7)$$

magneton, μ and m are the magnetic and electric moment operators, respectively, $\bar{D}_0(\Pi_u(j)) = -{}^1/_3\langle\Sigma_g^+||m^{\Pi_u}||\Pi_u(j)\rangle\langle\Pi_u(j)||m^{\Pi_u}||\Sigma_g^+\rangle$, the electric dipole strength of the $\Sigma_g^+ \rightarrow \Pi_u(j)$ transition, and $\Delta W_{kj} = W_k - W_j$, the energy difference between the states k and j. When the spin–orbit $|^{\Pi}_u(j)\rangle$ and $|\Sigma_u^+(j)\rangle$ states of eq 1 and 2 are substituted into eq 5–7, the resulting equations may be simplified to eq 8–10, where $m_z = \langle 2\sigma_g^+|m_z|2\sigma_u^+\rangle$ and

$$\bar{A}_1(\Pi_u(j)) = (|a_j|^2 + |b_j|^2 + 2|c_j|^2)|a_j|^2\,\bar{D}_0(^1\Pi_u) \quad (8)$$

$$\bar{B}_0(\Pi_u(j),\Pi_u(k)) = \sum_{k\neq j}\frac{-2}{\Delta W_{kj}}(a^*_j a_k + b^*_j b_k + 2c^*_j c_k)a_j a^*_k\,\bar{D}_0(^1\Pi_u) \quad (9)$$

$$\bar{B}_0(\Sigma_u^+(j),\Pi_u(k)) = \sum\frac{2}{3\Delta W_{kj}}(-2d^*_j b_k + d^*_j c_k + 2^{1/2}e^*_j a_k) \times e_j a^*_k(2(2^{1/2}))m_z(m_x + m_y) \quad (10)$$

$m_\gamma = \langle 2\sigma_g^+|m_\gamma|1\pi_u\gamma\rangle$, $\gamma = x$ or y. In the formulation of eq 8–10 the one-electron MO's were approximated by pure np halide and 6s Hg atomic orbitals and the summations in eq 9 and 10 were truncated to include only states within the $(1\pi_u)^3(2\sigma_g^+)$ and $(1\sigma_u^+)(2\sigma_g^+)$ or $(1\pi)^3(3\sigma^+)$ and $(2\sigma^+)(3\sigma^+)$ configurations, respectively, because contributions from all others will be much smaller due to larger ΔW_{kj} values. Equations 8–10 are sufficient to predict the sign of the MCD parameters, but in view of the approximations involved they are probably not adequate to give quantitative values. For example, the $\bar{D}_0(^1\Pi_u)$ and the m_x, m_y, and m_z integrals are two-centered, involving the Hg 6s and the halide np orbitals, and are not easily computed exactly. The value of $\bar{D}_0(^1\Pi_u)$ is certainly positive but may be quite small (see later); overlap considerations indicate m_z is positive but m_x and m_y are both negative with our choice of coordinate system and conventions.[22]

Spectral Assignment and MCD Interpretation. The spectra of HgI_2 and CH_3HgI reveal more features which are better resolved and located at lower energy than those of the bromo and chloro complexes. This latter observation is in accord with expectation for LMCT transitions: the spectra should exhibit the energy ordering $I^- < Br^- < Cl^-$ for corresponding transitions. The iodo complexes are also expected to be the most strongly influenced by ligand spin–orbit coupling, which should increase the complexity of the spectra, especially in the low-energy region, where transitions to states of triplet parentage are most easily observed. Therefore, the discussion here will center on the interpretation of the HgI_2 and CH_3HgI spectra, which will then provide the general framework for the spectra of the bromo and chloro complexes.

HgI_2. The earlier assignments of the low-energy bands in the $HgCl_2$ and $HgBr_2$ spectra, which were based on the relativistic

Table IV. Spin–Orbit Energies and Coefficients and MCD Parameters for HgI_2[a]

state	calcd energy, μm^{-1}	calcd $\bar{B}_0$[b]	calcd $\bar{A}_1$[c]	obsd MCD,[d] μm^{-1} ($\Delta\epsilon_M$, M^{-1} cm^{-1} T^{-1})	calcd coeff $a(^1\Pi_u)$	$b(^3\Pi_u)$	$c(^3\Sigma_u^+)$	$d(^3\Pi_u)$	$e(^1\Sigma_u^+)$
$\Pi_u(1)$	3.10	−0.64	+0.17		0.306	0.298	0.904		
$\Sigma_u^+(1)$	3.35	−8.18		3.25 (−0.88)				0.861	0.509
$\Pi_u(2)$	3.46	+9.44	+0.77	3.67 (+0.90)	−0.547	0.832	−0.892		
$\Pi_u(3)$	4.24	−8.60	+0.71	4.07 (−1.26)	0.779	0.468	−0.418		
$\Sigma_u^+(2)$	4.50	+7.98		4.50 (+1.16)				−0.509	0.861

[a] Input parameters (in μm^{-1}): $^1\Sigma_u^+ = 4.20$, $^3\Sigma_u^+ = 3.30$, $^1\Pi_u = 3.90$, $^3\Pi_u = 3.60$, $\zeta_{5p} = 0.50$. [b] Contributions from the sum of $\bar{B}_0(\Sigma_u^+(j),\Pi_u(k))$ in units of $|m_z(m_x + m_y)|$, μm; contributions from $\bar{B}_0(\Pi_u(j),\Pi_u(k))$ were small and were taken to be zero. [c] In units of $\bar{D}_0(^1\Pi_u)$. [d] From Table II; cyclohexane solution.

core potential MO calculations,[10] are not transferable to the HgI_2 spectra because ligand spin–orbit effects were neglected. For example, band I for $HgCl_2$ and $HgBr_2$ was assigned as $^1\Sigma_g^+ \rightarrow {}^1\Pi_u(1\pi_u \rightarrow 2\sigma_g^+)$ and band II was assigned as $^1\Sigma_g^+ \rightarrow {}^1\Sigma_u^+(1\sigma_u^+ \rightarrow 2\sigma_g^+)$. These simple assignments cannot account for the observed MCD since they would predict an A term for band I but only a B term for band II. Also, cogent arguments based on ground- and excited-state overlap considerations predict the intensity of $1\sigma_u^+ \rightarrow 2\sigma_g^+$, a $\sigma \rightarrow \sigma^*$ type LMCT transition, to be much larger than that of $1\pi_u \rightarrow 2\sigma_g^+$, a $\pi \rightarrow \sigma^*$ type transition. The oscillator strength for band II was calculated[10] to be 10-fold greater than for band I for both $HgCl_2$ and $HgBr_2$. For HgI_2 the integrated intensity for band II is found to be only 1.6 ± 0.4 times that for band I, which suggests considerable intensity enhancement for band I. The failure of simple intensity arguments can also be a consequence of extensive mixing of states by spin–orbit coupling.

In order to characterize the ligand spin–orbit effects in HgI_2 and to provide explanations for both the absorption intensity and the MCD pattern, some simple spin–orbit computations were performed. The determinants of eq 3 and 4 were diagonalized to obtain energies and eigenvectors (eq 1 and 2) for both the Σ_u^+ and Π_u spin–orbit states of Table III. The eigenvector coefficients were then used in eq 8–10 to calculate parameters for the MCD terms for each of these states. The results of a typical calculation, together with input energies for the singlet and triplet zero-order states, are summarized in Table IV. The choice of input energies for the singlet and triplet states in the absence of spin–orbit coupling was guided by the earlier MO results for $HgCl_2$ and $HgBr_2$,[10] but the calculated results were rather insensitive to small variations in the input energies. The results in Table IV were not extensively optimized to provide a precision quantitative spectral fit, but they do reveal several interesting features. First, the presence of the three states $\Pi_u(1)$, $\Sigma_u^+(1)$, and $\Pi_u(2)$ at energies near that of band I of HgI_2 may account for some of the broadness of the band. However, the $^1\Sigma_u^+$ character in $\Sigma_u^+(1)$ (~25%) can clearly provide considerable intensity for band I, even though this state is derived from $^3\Pi_u$. Second, the calculated B_0 parameters derived from the magnetic interaction of the $\Sigma_u^+(j)$ and $\Pi_u(k)$ states are in accord with the sign pattern and relative intensity in the observed MCD spectra. The contribution from B terms due to the interaction between the $\Pi_u(j)$ and $\Pi_u(k)$ states was found to be small. The A-term contributions to the MCD from the $\Pi_u(j)$ states is also expected to be small on the basis of the intensity arguments noted above ($\bar{D}_0(^1\Pi_u)$ is expected to be small). Even so, the close placement of the pairs of states $\Sigma_u^+(1)$–$\Pi_u(2)$ and $\Sigma_u^+(2)$–$\Pi_u(3)$ gives rise to two positive pseudo A terms composed of B terms of similar magnitude and opposite sign.[22] The A terms expected for $\Pi_u(2)$ and $\Pi_u(3)$, which have the largest $^1\Pi_u$ character, are both positive and will simply enhance to some small extent the positive and negative observed MCD in the region of bands I and II. It seems unlikely that the A terms could be separately resolved from the large B terms. Similarly the small negative B term and small positive A term expected for $\Pi_u(1)$, together with a low absorption intensity, would preclude resolution from the more intense $\Sigma_u^+(1)$ features. Thus, the spin–orbit results of Table IV lead to the conclusion that the absorption band intensity for bands I and II is carried primarily by the $^1\Sigma_u^+$ character of $\Sigma_u^+(1)$ and $\Sigma_u^+(2)$ but that the MCD requires the presence of both Σ_u^+ and Π_u spin–orbit states and is dominated by their B terms which give the appearance of two positive pseudo A terms.

The interpretation of band II of HgI_2 as $\Sigma_u^+(2)$, which is predominantly $^1\Sigma_u^+(1\sigma_u^+ \rightarrow 2\sigma_g^+)$, provides a rationale for the vibrational structure observed in this band in the vapor-phase spectrum (Figure 1). From MO calculations on $HgCl_2$[10] the $^1\Sigma_u^+$ state is predicted to be nonlinear with a minimum energy corresponding to a bond angle of ~80–120°. An analogous nonlinear state is expected for HgI_2. Therefore, the long progression in bending vibration observed on the low-energy side of band II is reasonable in the Franck–Condon approximation if the $^1\Sigma_u^+$ excited state prefers a nonlinear structure while the $^1\Sigma_g^+$ ground state is linear. The vibrational structure thus strongly indicates the presence of a bound HgI_2 molecular state, but the low resolution of the structure and the overall broadness of band II also suggests an underlying dissociative excitation. The $^1\Sigma_u^+$ state correlates with $HgI(B^2\Sigma^+) + I(^2P_{3/2})$ energetically at ~4.5 μm^{-1}.[10,15] The broadness of band II, especially on the high-energy side, is therefore consistent with the HgI + I potential surface crossing that of the $^1\Sigma_u^+$ HgI_2 excited state. Excitation of HgI_2 in the energy region of band II is known to produce HgI (B → X) emission at 2.43 μm^{-1}.[10,15]

The large width of band I (0.45–0.50 μm^{-1} in both vapor phase and solution) is consistent with contributions from several unresolved transitions. In addition to the allowed $\Sigma_u^+(1)$, $\Pi_u(1)$, and $\Pi_u(2)$ spin–orbit states discussed above, states of the parity-forbidden $(1\pi_g)^3(2\sigma_g^+)$ excited configuration are also expected in the energy region of band I. Transitions to the spin–orbit states of $^1\Pi_g$ and $^3\Pi_g$ could also contribute to the intensity and width of band I by vibronic coupling to the nearby allowed states. However, the lack of resolution of individual features precludes a more detailed discussion of the intensity distribution in band I via a vibronic mechanism.

The structured band III and the unstructured band IV in the vapor-phase spectrum of HgI_2 are more difficult to interpret from our present results because these bands are not separately resolved in the solution MCD spectra. Their position at energies higher than that of band II and their lower relative intensity are consistent with transitions to states of configurations involving $2\pi_u$ and are likely states of spin-forbidden parentage. There are three Σ_u^+ and four Π_u spin–orbit states expected from the $(1\pi_g)^3(2\pi_u)$ and $(1\sigma_g^+)(2\pi_u)$ configurations, and both I^- and Hg spin–orbit coupling will be important. The lowest energy states of the $(1\pi_g)^3(2\pi_u)$ configuration are expected to be $\Sigma_u^+(^3\Sigma_u^-)$, $\Pi_u(^3\Sigma_u^-)$, and $\Pi_u(^3\Sigma_u^+)$. The transition to the Σ_u^+ state is likely to be the most intense because the only allowed singlet state of the $(1\pi_g)^3(2\pi_u)$ configuration is $\Sigma_u^+(^1\Sigma_u^+)$. The Π_u states can only gain intensity from a $^1\Pi_u$ state from the higher energy $(1\sigma_g^+)(2\pi_u)$ configuration. In contrast to the case for the lower energy states of the $(1\pi_u)^3(2\sigma_g^+)$ and $(1\sigma_u^+)(2\sigma_g^+)$ configurations, the states of $(1\pi_g)^3(2\pi_u)$ are expected to prefer linear geometry.[10] Linear excited-state geometry may explain why the structure in band III involves the symmetric Hg–I stretch rather than the bending mode. A tentative assignment of band III is to the transition to $\Sigma_u^+(^3\Sigma_u^-)$ on the basis of its intensity and expected energy under the influence of spin–orbit coupling. Band IV may be due to either $\Pi_u(^3\Sigma_u^-)$ or $\Pi_u(^3\Sigma_u^+)$, and the broad unresolved absorption between bands III and IV may signal the presence of the other.

CH_3HgI. Bands I and III in the CH_3HgI vapor-phase absorption spectrum (see Figure 1), although shifted 0.5 μm^{-1} to higher energy, appear to be analogous to bands I and II for HgI_2 both in energy separation and relative intensity. Therefore, these bands are logically interpreted as due to transitions to the I^- to Hg 6s LMCT spin–orbit states of $(1\pi)^3(3\sigma^+)$ and $(2\sigma^+)(3\sigma^+)$, which are exactly analogous to those of $(1\pi_u)^3(2\sigma_g^+)$ and $(1\sigma_u^+)(2\sigma_g^+)$ discussed above for HgI_2 (see Table III). The blue shift of the LMCT states can be understood in terms of ligand donor strength: When the weaker σ-donor I^- ligand is replaced by the stronger σ-donor CH_3^- ligand, the σ^* Hg 6s orbital $2\sigma_g^+$ (Figure 4) in HgI_2 will be destabilized to $3\sigma^+$ in CH_3HgI. The I^--based 1π and $2\sigma^+$ orbitals are expected to be relatively insensitive to the replacement. The vibrational structure in band III of CH_3HgI parallels that in band II of HgI_2 but is better resolved. The progression in the CH_3–Hg–I bending mode consistent with a nonlinear Σ^+ spin–orbit state indicates the transition is to a bound molecular state at energies in the region of band III to just beyond the maximum. On the high-energy side of band III the structure becomes considerably less well resolved, suggesting a CH_3Hg + I dissociative excitation. It is interesting that some weak vibrational structure (also in the bending mode) appears in the center of band I, where the transition to the $\Sigma^+(^3\Pi)$ spin–orbit state is expected. The resolution of structure in band I for CH_3HgI and the absence of structure in band I for HgI_2 may be due to the presence of the additional parity-forbidden vibronic transitions in the case of HgI_2. However, band I is very broad in both cases and must encompass transitions to several states as discussed above. The MCD spectrum for band I of CH_3HgI (Figure 3) is also very similar to that for band I of HgI_2 and shows the same positive pseudo-*A*-term pattern. The MCD for band III of CH_3HgI is incomplete because of solvent cutoff, but the negative *B* term appears analogous to the negative *B* term below the band II maximum for HgI_2. Thus, the correspondence between bands I and III for CH_3HgI and bands I and II for HgI_2, respectively, in both absorption and MCD is striking and gives credibility to a parallel interpretation.

Band II, which is clearly resolved in the vapor-phase spectrum of CH_3HgI and is probably responsible for the MCD *A* term centered at 4.67 μm^{-1} and the broadness on the low-energy side of the band at 4.97 μm^{-1} in the solution absorption spectrum (Figure 3), is a feature outside of the spin–orbit model applied to bands I and III and also has no parallel between bands I and II for HgI_2. A reasonable approach to the interpretation of band II for CH_3HgI is to consider a transition to a state of the next lowest energy excited configuration, which is assumed to be $(1\pi)^3(2\pi)$, I^- to Hg 6p π LMCT. Since the replacement of a π-donor I^- ligand in HgI_2 by the non-π-bonding CH_3^- will reduce the overall π interaction in CH_3HgI compared to that in HgI_2, the antibonding 2π orbital (Figure 4) of CH_3HgI would be expected to be lower in energy than the corresponding $2\pi_u$ orbital of HgI_2. This would have the effect of lowering the I^- to Hg 6pπ LMCT energies. Therefore, band II of CH_3HgI is assigned to a transition to a Π or Σ^+ spin–orbit state from the $(1\pi)^3(2\pi)$ configuration, which would be analogous to bands III or IV for HgI_2 but shifted slightly to the red due to the lower π interaction in CH_3HgI. The positive *A* term in the MCD argues for a Π state, but a pseudo *A* term resulting from a Σ^+ and a Π state close in energy is also a possibility. Band II for CH_3HgI is unstructured whereas band III in HgI_2, assigned as $\Sigma_u^+(^3\Sigma_u^-)$, is structured and band IV in HgI_2, assigned as either $\Pi_u(^3\Sigma_u^-)$ or $\Pi(^3\Sigma_u^+)$, is not. On the basis of parallel assignments in the two complexes one of the two Π states, either $\Pi(^3\Sigma^-)$ or $\Pi(^3\Sigma^+)$, is favored for band II of CH_3HgI. Both of these states are predicted to have positive *A* terms; therefore, the present results do not provide a basis for deciding between them.

Finally, the structured rising absorption at high energy in the vapor-phase spectrum (band IV, Table I) exhibits a Hg–I stretching progression that suggests an intense transition to a linear excited state. The lowest energy predominantly spin allowed state of the $(1\pi)^3(2\pi)$ configuration is $\Sigma^+(^1\Sigma^+)$, and a transition to this state is suggested. The corresponding state for HgI_2 is assumed to be higher in energy beyond the range of measurement.

$HgBr_2$ and $HgCl_2$. The experimental spectra for $HgBr_2$ and $HgCl_2$ reveal fewer features than the spectra for HgI_2 in the region accessible to our measurements. This is a natural consequence of the blue shift of the LMCT expected as the stability of the highest energy halide orbitals increases from I^- to Cl^-. Two band systems, each found $\sim$0.6 μm^{-1} higher in energy than bands I and II for HgI_2, were observed in the vapor-phase spectrum for $HgBr_2$, but only the lowest energy band was observed for $HgCl_2$ $\sim$0.63 μm^{-1} higher in energy than band I for $HgBr_2$ (Table I).

The spin–orbit model used for HgI_2 should still be applicable to $HgBr_2$ because even though the coupling constant ζ_{4p} for Br^- is a little less than half of the ζ_{5p} value for I^- it is still significant (0.25 μm^{-1}). The consequence of lower ligand spin–orbit coupling is a lower spin–orbit splitting of the Σ_u^+ and Π_u spin–orbit states (Table III) and reduced intermixing of singlet and triplet zero-order states. The decrease in spin–orbit interaction provides an explanation for the lower relative intensity of band I compared to that of band II for $HgBr_2$ (estimated to be $\sim$0.2 vs 0.6 for HgI_2) because of the $^1\Sigma_u^+$ character in $\Sigma_u^+(^3\Pi_u)$ will be less. The lower spin–orbit splitting can also be used to explain the change in shape of the MCD for $HgBr_2$ in the region of band I compared to that for HgI_2. A lower separation between the spin–orbit states associated with band II ($\Sigma_u^+(^1\Sigma_u^+)$ and $\Pi_u(^1\Pi_u)$) and those associated with band I ($\Pi_u(^3\Sigma_u^+)$, $\Sigma_u^+(^3\Pi_u)$, and $\Pi_u(^3\Pi_u)$) may be visualized as resulting in a compression of the MCD features for $HgBr_2$ on the energy axis—the middle positive and negative *B* terms, resolved separately for HgI_2 (see Figure 2), are expected to overlap significantly with a near-cancellation of the positive portion of the MCD between the two absorption bands.

The parallel interpretation of bands I and II for $HgBr_2$ and HgI_2 is also strengthened by the observation of weak vibrational structure on band II in the vapor-phase spectrum of $HgBr_2$, reminiscent of the structure observed on band II for HgI_2. The structure on band II for $HgBr_2$ is very poorly resolved but seems to be a progression in the symmetric Hg–Br stretch in contrast to the long bending mode progression on band II for HgI_2. It must be admitted that the low resolution and few identifiable vibrational components for $HgBr_2$ limit the reliability of the vibrational mode assignment. Better data are required before a difference between the vibrational structure between $HgBr_2$ and HgI_2 can be confirmed.

Little detail can be inferred from the absorption and MCD spectra of band I for $HgCl_2$ except to note that the MCD follows the pattern of a negative minimum below the energy of the first absorption band established for HgI_2 and $HgBr_2$. The low spin–orbit coupling due to ζ_{3p} for Cl^- (0.06 μm^{-1}) would suggest that the spin–orbit model is unnecessary and the interpretation could be based on transitions to zero-order singlet states. If so, the transition $^1\Sigma_g^+ \rightarrow {}^1\Pi_u(1\pi_u \rightarrow 2\sigma_g^+)$ is predicted to be the lowest energy transition and is expected to be considerably weaker than the high-energy $^1\Sigma_g^+ \rightarrow {}^1\Sigma_u^+(1\sigma_u^+ \rightarrow 2\sigma_g^+)$ transition (observed in the vacuum-UV region).[10]

CH_3HgBr and CH_3HgCl. The two bands observed in the vapor-phase spectrum for CH_3HgBr are analogous to bands I and III for CH_3HgI but are shifted 0.25–0.38 μm^{-1} to higher energy. Thus, the spin–orbit LMCT model applied to bands I and III for CH_3HgI is applicable to the interpretation of bands I and II for CH_3HgBr. Band II for CH_3HgBr is structured like that of band III for CH_3HgI, but the resolution is lower and fewer components are clearly visible. Both the bending mode and Hg–Br stretching mode are identified in the structure of band II for CH_3HgBr in contrast to the long progression in the bending mode observed in band III for CH_3HgI. This difference in vibrational structure between the iodo and bromo complexes parallels that noted above for HgI_2 and $HgBr_2$, but in view of the quality of the data for CH_3HgBr (and $HgBr_2$) it is probably unwise to speculate as to its origin. Finally, there is no evidence in the CH_3HgBr spectrum for a band analogous to band II for CH_3HgI. It is probable that this transition has also suffered a blue shift and lies unresolved beneath the intense band II. Also, the MCD spectrum for CH_3HgBr (Figure 3) is not complete enough to be helpful, al-

though as far as the data go they do parallel the MCD data for $HgBr_2$ as expected.

The absorption spectrum of CH_3HgCl did not reveal any well-defined bands below 5.2 μm^{-1}, either in solution or in the vapor phase. This observation is consistent with the blue shift of the lowest energy band compared to that for CH_3HgBr predicted for LMCT. A blue shift from the bands of $HgCl_2$, where the lowest energy band is 4.9–5.0 μm^{-1}, is also expected so that the lack of an observed band in the measurement region here is quite reasonable.

Conclusions. The absorption and MCD spectra for bands I and II for HgI_2 and for bands I and III for CH_3HgI can be interpreted in a self-consistent and satisfactory way by the $I^- \rightarrow Hg$ 6s LMCT model, which includes the effects of I^- spin–orbit coupling. The relative absorption intensity is ascribed to the singlet character in the Σ_u^+ or Σ^+ spin–orbit states, but the explanation of the pseudo A terms in the MCD spectra requires close-lying Σ_u^+ and Π_u or Σ^+ and Π spin–orbit states. The observed blue shift of the CH_3HgI spectra relative to the HgI_2 spectra is expected within the model because of the stronger σ-donor strength of the CH_3^- ligand compared to that of I^-. The long progressions in the bending vibrations that structure band II for HgI_2 and bands I and III for CH_3HgI provide a strong indication of bound molecular excited states for the LMCT, which are bent and therefore Franck–Condon-shifted relative to the linear ground states. However, the underlying broadness of each of the LMCT bands also suggests the possibility of a dissociative potential surface crossing that of the bound state in the energy region of the band maximum and beyond.

Although the data are not as extensive and the individual features are not as well-resolved, the spectra for $HgBr_2$ and CH_3HgBr follow the LMCT pattern in the iodo complexes, except, as expected, shifted to higher energy. The difference in the MCD spectra, together with the changes in the relative intensities for the LMCT bands for the bromo complexes compared to those for the iodo complexes, is compatible with that expected from the lower excited state spin–orbit interaction from Br^- compared to that from I^-. Little detail can be extracted from the spectra of $HgCl_2$ and CH_3HgCl because of the LMCT blue shift to the edge of our measurement capability or beyond.

Acknowledgment. Helpful discussions with Dr. C. T. Lin are gratefully acknowledged.

Registry No. HgI_2, 7774-29-0; $HgBr_2$, 7789-47-1; $HgCl_2$, 7487-94-7; CH_3HgI, 143-36-2; CH_3HgBr, 506-83-2; CH_3HgCl, 115-09-3.

Contribution from the Department of Chemistry,
The University of Calgary, Calgary, Alberta, Canada T2N 1N4

Pressure Effects on the Rates of Electron Transfer between Tris(hexafluoroacetylacetonato)ruthenium(II) and -(III) in Different Solvents

Hideo Doine and Thomas W. Swaddle*

Received June 18, 1987

Rate constants k for electron transfer between $Ru(hfac)_3^-$ and $Ru(hfac)_3^0$ in the perdeuteriated solvents acetone, acetonitrile, chloroform, and methanol have been measured as functions of pressure up to 200 MPa by ^1H NMR spectroscopy. Development of the Stranks–Hush–Marcus (SHM) theory indicates, and the data for methanol confirm, that ln k is a nonlinear function of pressure, but approximation to linear dependence gives the mean experimental ΔV^* values −6 ($(CD_3)_2CO$), −5.5 (CD_3CN), −8.1 ($CDCl_3$), and −5.8 $cm^3\ mol^{-1}$ (CD_3OD). For chloroform and methanol, respectively, $\Delta H^* = 24.5$ and 22 (±3) kJ mol^{-1} and $\Delta S^* = -28$ and −41 J K^{-1} mol^{-1}. Ion pairing with the tetra-*n*-butylammonium counterion appears to dominate the kinetics in chloroform. In the other solvents, the kinetics are consistent with adiabatic SHM theory with predominant contributions from solvent reorganization and a secondary contribution (amounting to some 16 kJ mol^{-1} in ΔG^* but only +1 ± 1 $cm^3\ mol^{-1}$ in ΔV^*) from internal reorganization within the Ru complexes. The pressure dependence of the ^1H line width and chemical shift of tris(acetylacetonato)chromium(III) in the four solvents is also reported.

Introduction

We report here an extension of our continuing studies of the effects of pressure on electron-transfer (ET) kinetics in solution to cover solvents other than water. As comparison of the gas- and solution-phase rates of intermolecular ET reactions of metallocene–metallocenium couples clearly shows,[1] the kinetics of ET reactions can be markedly influenced by solvent effects,[2] which in turn are sensitive to applied pressure. Stranks[3] attempted to develop the classical Hush[4] (cf. Marcus[2]) ET theory to account for the effect of pressure (expressed as the volume of activation ΔV^*) on outer-sphere ET rates but was less successful than at first appeared because of an error in treating the contribution from medium (Debye–Hückel) effects.[5]

An adaptation of Stranks' approach[6] can, however, account quite accurately for the experimental ΔV^* as well as the enthalpy ΔH^* and entropy ΔS^* of activation for the cation-independent pathway for ET between manganate and permanganate ions in aqueous solution. Unfortunately, we have been unsuccessful in attempts to extend our ^{55}Mn-NMR-based kinetic studies of this reaction to nonaqueous solvents; only aprotic solvents can be considered, and most organic solvents (or impurities in them) tend to reduce one or both of the reactants, and the solubility of salts of the manganate ion in particular is often insufficient for the NMR measurements even in the presence of 18-crown-6.[7]

We have therefore turned our attention to the $Ru^{II}(hfac)_3^-$–$Ru^{III}(hfac)_3^0$ self-exchange reaction (hfac = 1,1,1,5,5,5-hexafluoropentane-2,4-dionate), which has been studied by Chan and Wahl[8] in several perdeuteriated organic solvents by measurement of the effect of small amounts of the Ru^{III} complex upon the ^1H and ^{19}F NMR line widths of the diamagnetic Ru^{II} partner. Although this system cannot be studied in water, it offers several advantages. The electrical neutrality of the Ru^{III} complex makes it unnecessary to consider ionic medium effects or the Coulombic work terms involved in bringing the reactants together, and (in contrast to the MnO_4^-–MnO_4^{2-} case) there is no detectable reaction pathway involving the counterion of the Ru^{II} complex.[8] The reactant molecules are large, so that a "two-sphere" theoretical model that treats the solvent as a continuous dielectric should suffice (again, in contrast to the case of the small MnO_4^-–MnO_4^{2-} ions).[6] Chan and Wahl point out[8] that the contribution of internal rearrangement[2-4,6] of the reactants to the reaction rate is not large, and (more importantly, for our purposes) Stranks[3] showed that

(1) Eyler, J. R.; Richardson, D. E. *J. Am. Chem. Soc.* **1985**, *107*, 6130.
(2) Marcus, R. A. *J. Chem. Phys.* **1956**, *24*, 966, 979; **1957**, *26*, 867.
(3) Stranks, D. R. *Pure Appl. Chem.* **1974**, *38*, 303.
(4) Hush, N. S. *Trans. Faraday Soc.* **1961**, *57*, 557.
(5) Wherland, S. *Inorg. Chem.* **1983**, *22*, 2349.
(6) Spiccia, L.; Swaddle, T. W. *Inorg. Chem.* **1987**, *26*, 2265; *Physica B+C (Amsterdam)* **1986**, *139/140B+C*, 684.
(7) Bock, H.; Jaculi, D. *Angew. Chem., Int. Ed. Engl.* **1984**, *23*, 305.
(8) Chan, M. S.; Wahl, A. C. *J. Phys. Chem.* **1982**, *86*, 126.

0020-1669/88/1327-0665$01.50/0